Resonant Auger decay of iodobenzene below the I 4d edge

Stephen T Pratt, Ugo Jacovella, Bérenger Gans, John D Bozek, David M P Holland

The Journal of Chemical Physics

AIP Publishing

RESONANT AUGER DECAY OF IODOBENZENE BELOW THE I 4d EDGE

Stephen T. Pratt,[a]* Ugo Jacovella,[b] Bérenger Gans,[b] John D. Bozek,[c]

and David M. P. Holland[d]

[a]Chemical Sciences and Engineering Division, Argonne National Laboratory, Lemont, IL 60439 USA

[b]Institut des Sciences Moléculaires d'Orsay, CNRS, Université Paris-Saclay, F-91405 Orsay, France

[c]Synchrotron SOLEIL, l'Orme des Merisiers, Départmentale 128, 91190 Saint-Aubin, France

[d]STFC, Daresbury Laboratory, Daresbury, Warrington, Cheshire, WA4 4AD, UK

*Corresponding Author Email: stpratt@anl.gov

ABSTRACT

New data are presented on the resonant Auger decay of iodobenzene (C_6H_5I) in the region of the I $4d^{-1}$ ionization threshold. The excited molecules decay by participator and spectator processes to populate single-hole valence states and two-hole, one-particle excited states of the cation, providing new information on the structure of $C_6H_5I^+$. Excitation of dissociative C_6H_5I (I $4d_{5/2,3/2}^{-1}$)σ* resonances can in principle result in ultrafast dissociation to C_6H_5 + I** and the subsequent autoionization of I**, but no evidence for this process is observed. The results are compared with our recent study of the resonant Auger decay of methyl iodide (CH_3I).

Keywords: iodobenzene, photoelectron spectroscopy, resonant Auger Decay, ultrafast dissociation

I. INTRODUCTION

The excited states produced by resonant excitation near a core-ionization threshold can decay by a number of competing ionization, dissociation, and fluorescence processes, as well as by more complex sequences of these processes.[1,2,3,4,5] This competition provides a unique probe of electron correlation, the coupling of electronic and nuclear motion, and the structure of atomic and molecular ions. The autoionization of such resonantly excited states via Auger processes can proceed via two general mechanisms.[6,7,8] If the electron in the resonantly excited orbital is directly involved in the ionization process, it is called participator decay. This process generally results in the production of single-hole states of the ion. If, however, the excited electron is not directly involved in the decay process, it is called spectator decay, and results in two-hole, one-particle states of the cation. Such states are typically not accessed in single-photon valence photoelectron spectroscopy[9] because they require two-electron transitions that tend to be weak. Electron correlation and relaxation effects can complicate this simple picture, resulting in "shake-up" and "shake-down" processes and more complex electron dynamics.

In the present paper, we focus on resonant Auger processes in iodobenzene (C_6H_5I) in the region just below the I ($4d_{5/2,3/2}^{-1}$) thresholds, and compare these with our recent results on the analogous processes in CH_3I.[10] The dominant features in the C_6H_5I absorption spectrum in this region correspond to transitions from the ground electronic state to the C_6H_5I (I $4d_{5/2,3/2}^{-1}$)σ^* resonances, where the σ^* orbital is the antibonding LUMO. Somewhat weaker transitions are also observed to Rydberg states converging to the I $4d^{-1}$ thresholds. The differences between the C_6H_5I and CH_3I decay processes result from two principal effects. First, the phenyl group is a better electron donor than the methyl group, so that the resonances and thresholds due to I 4d excitation and ionization are shifted to lower energy. Second, for neutral dissociation processes, the heavier phenyl group results in the slower separation of the two fragments along the dissociation coordinate. As a result, ultrafast dissociation[11,12,13] is expected to be less important for C_6H_5I than for CH_3I.

In what follows, we briefly describe the experimental apparatus and approach to the data analysis, and follow this with a discussion of the results. As in our previous paper on CH_3I, we focus primarily on the lowest energy participator and spectator Auger processes.

II. EXPERIMENT

The experiments were performed at the PLEIADES undulator beamline of the Synchrotron SOLEIL[14] following the approach described in our recent paper on resonant Auger processes near the I 4d edge of CH_3I. The details of the undulator, beamline, and end station have been described previously,[14] and only a few relevant details are discussed here.

Vapor from a room temperature sample of iodobenzene was introduced through a leak valve into a differentially pumped gas cell. All of the spectra were recorded within a small range of photon energies (50 – 60 eV), and the photon energy was calibrated by using the spectrum of atomic Ne in the same energy range.[15,16] The electron kinetic energies were calibrated by using the known energies of features within the $C_6H_5I^+ \tilde{X}\,^2B_1 \leftarrow C_6H_5I\,\tilde{X}\,^1A_1$ band.[17] The photon energy resolution and electron energy resolution were determined to be ~ 0.007 eV and 0.047 eV, respectively, and the calibration of the photon energies and electron kinetic energies is accurate to better than ± 5 meV and ±10 meV, respectively. The transmission of the electron spectrometer is relatively independent of electron kinetic energies over the range of interest, and the intensities were not corrected for any such dependence.

Photoelectron spectra were recorded for both the parallel (0°) or perpendicular (90°) geometry of the linearly polarized light relative to the detection axis of the electron spectrometer. The well-known formula:[18,19,20]

$$\frac{d\sigma}{d\Omega} = \frac{\sigma}{4\pi}[1 + \beta P_2(\cos\theta)] \quad , \qquad (1)$$

gives the angular distribution of the photoelectrons in the electric dipole approximation. Here, σ is the angle-integrated cross section, β is the angular distribution parameter, $P_2(\cos\theta) = (3\cos^2\theta - 1)/2$, and θ is the angle between the polarization axis of the light and the detection axis of the electron spectrometer. The electron intensities at 0° and 90° can be used to derive the value of β using:[21]

$$\beta = \frac{2(I_0 - I_{90})}{(I_0 + 2I_{90})} \quad , \tag{2}$$

and the total cross section ("magic-angle" photoelectron spectrum) is proportional to:

$$\sigma \propto \frac{(I_0 + 2I_{90})}{3} \ . \tag{3}$$

For the photoelectron angular distributions, the electron signals at 0° and 90° were scaled by using an average value of the relative photon fluxes for the two undulator polarizations. The resulting β values for the first six valence bands at photon energies around 50 eV are in reasonable agreement with the values reported previously by Holland et al.[17]

Molecular orbitals for ground state neutral iodobenzene were obtained at the M062X/MidiX level of theory using Gaussian16[22] and visualized using the Avogadro software package.[23,24]

III. RESULTS AND DISCUSSION

Figure 1 shows the photoelectron spectrum of iodobenzene in the region of the I $4d^{-1}$ thresholds at a photon energy of 120 eV and $\theta = 0°$. The two peaks correspond to transitions to the $C_6H_5I^+$ (I $4d^{-1}$) $^2D_{5/2}$ and $^2D_{3/2}$ thresholds, yielding values of 56.49 ± 0.010 and 58.203 ± 0.010 eV, respectively. In the ligand field of the molecule, the I $4d^{-1}$ $^2D_{5/2}$ and $^2D_{3/2}$ peaks split into three and two components, respectively, but these splittings are not resolved in the present experiments. The observed values are ~0.2 eV lower than the corresponding values for CH_3I.[25]

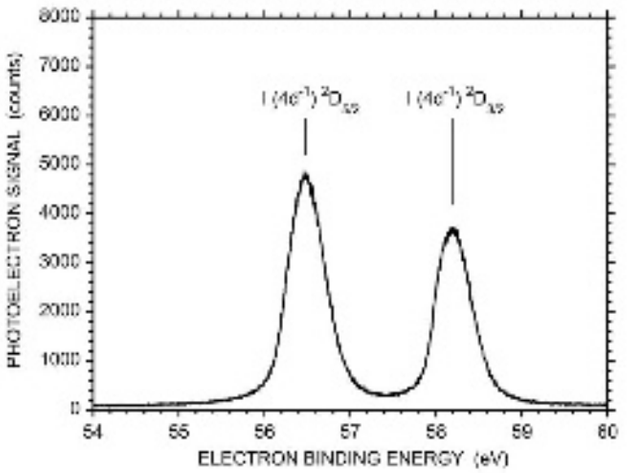

Figure 1. The photoelectron spectrum of iodobenzene in the region of the I 4d threshold, recorded at a photon energy of 120 eV by using linearly polarized light with $\theta = 0^o$.

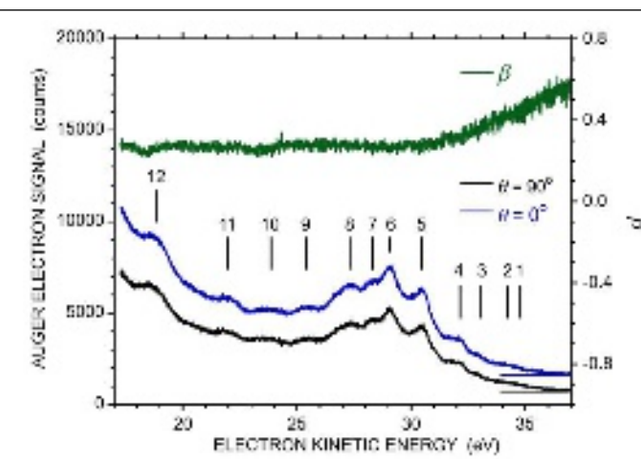

Figure 2. The Auger electron spectra of iodobenzene following 4d ionization at a photon energy of 137.5 eV for $\theta = 0^o$ and 90°. The β angular distribution parameter calculated using Equation 2 is also shown, where the error bars from counting statistics correspond to less than ±0.03. Background levels have been added to highlight the signal at points 1 and 2.

Figure 2 shows the normal Auger spectrum of $C_6H_5I^+$ taken following photoionization at 137.5 eV for both $\theta = 0^o$ and 90°. The electron energies were calibrated using the Auger electrons from Xe $4d^{-1}$ decay.[26] The energies of the numbered features are given in Table 1, but a detailed assignment of the spectrum is not possible at this time. However, the feature with the highest kinetic energy should come from the decay of $C_6H_5I^+$ (I $4d_{3/2}^{-1}$) at 58.203 eV, and this feature provides an upper limit to the C_6H_5I double photoionization threshold to form $C_6H_5I^{2+}$. The first numbered label in Figure 2 corresponds to the energy at which the Auger electron signal rises significantly above the background, and yields an upper limit of the double ionization threshold of (58.203 – 34.777 =) 23.426 eV. This value is consistent with values reported for CH_3I, C_3H_5I, and $C_6H_5CH_3$.[27] Figure 2 also shows the β parameter for the Auger electron spectrum. The error bars on β due to counting statistics alone are less than ±0.03 throughout the range of electron kinetic energies. The behavior of the β parameter is similar to that observed for $4d^{-1}$ Auger

Table 1. Auger-Electron Kinetic Energies Following Ionization from the I 4d Shell of Iodobenzene.

Peak #	Energy (eV)[a]
1	34.777[b]
2	34.240
3	32.896
4	32.188
5	30.497
6	29.061
7	28.292
8	27.279
9	25.437
10	23.861
11	22.017
12	18.840

(a) The uncertainty in the peak energies is ±0.005 eV.
(b) The slow rise does not result in a distinct peak, but the signal at this energy rises significantly above the background.

decay in CH_3I^+.[28] In particular, the β value is small across the lower range of Auger electron energies, then rises substantially at higher kinetic energies.

The total ion yield scan of iodobenzene in the region just below the I ($4d^{-1}$) thresholds is shown in Figure 3. The yield has been corrected for the photon flux, and the peak positions and assignments are given in Table 2. There is a strong continuum signal throughout this region due to direct photoionization of the valence shell, and the resonant structures are only ~5 – 20% of the intensity of this continuum. The assignments have been made by analogy with the methyl iodide spectrum,[28] but the present spectrum is somewhat less resolved. The energies of the C_6H_5I (I $4d_{5/2}^{-1}$)σ* and (I $4d_{3/2}^{-1}$)σ* resonances are ~0.2 to 0.3 eV higher than the corresponding resonances in CH_3I.

A. Participator Decay Processes

Figure 4 shows the photoelectron spectra of C_6H_5I on and off the (I $4d_{5/2}^{-1}$)σ* resonance. The off-resonance spectrum recorded at 49.966 eV is very similar to that recorded at 51.792 eV, midway

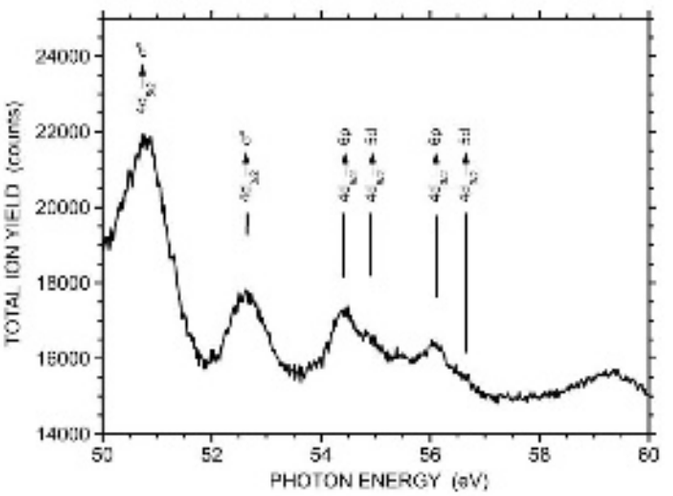

Figure 3. The total ion yields from iodobenzene in the region of the I 4d ionization threshold. The ion signal has been corrected by the photon intensity to account for the changing photon flux across this region.

Table 2. Transition Energies from the I 4d Shell of Iodobenzene.

Upper State	Energy (eV)
$(4d_{5/2}^{-1})\sigma^*$	50.80
$(4d_{3/2}^{-1})\sigma^*$	52.62
$(4d_{5/2}^{-1})6pe + 6pa_1$	54.41
$(4d_{5/2}^{-1})5d$	54.86
$(4d_{3/2}^{-1})6pe + 6pa_1$	56.06
$(4d_{3/2}^{-1})5d$	56.65
C_6H_5I (I $4d^{-1}$) thresholds	
I $^2D_{5/2}$	56.49 ± 0.01
I $^2D_{3/2}$	58.20 ± 0.01

between the two $(4d^{-1})\sigma^*$ resonances. At both energies, the contribution to the electron spectrum from the resonant processes is small. The spectra look quite similar up to electron binding energies of ~16 eV, but at higher energies some new features and differences begin to appear. The iodobenzene resonances excited below the I $4d^{-1}$ threshold can decay by participator and spectator processes. While participator processes access valence states of $C_6H_5I^+$ down to the ground state cation, spectator processes access two-hole, one-particle excited states that lie at somewhat higher energy. By analogy with CH_3I,[10] the lowest energy two-hole, one-particle states of C_6H_5I are expected to lie ~10 – 11 eV below the double ionization threshold, that is, at a binding energy of ~12 eV or higher. Below this energy, only participator processes are energetically allowed, and we consider this region first.

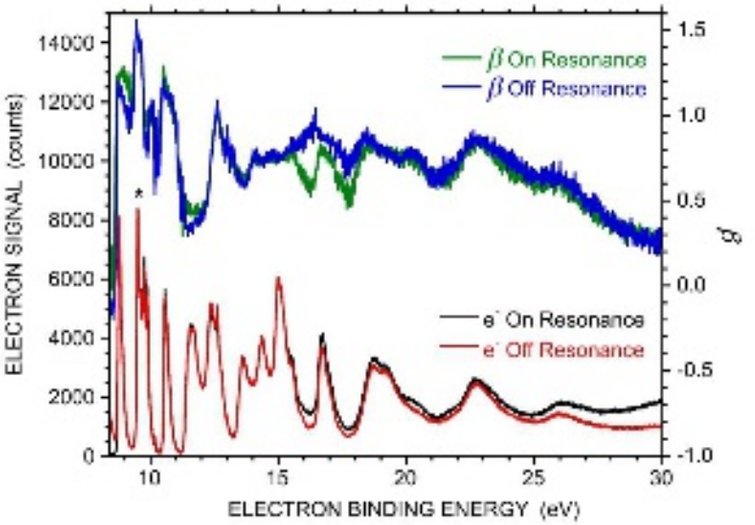

Figure 4. Overview of the magic-angle photoelectron spectra and electron angular distribution parameters following excitation on and off the iodobenzene (I $4d_{5/2}^{-1}$)σ* resonance at 50.797 eV and 49.966 eV, respectively. The magic angle spectra were determined by using Equation 3, and were normalized on the intensity of the $\widetilde{A}\,^2A_2 \leftarrow \widetilde{X}\,^1A_1$ origin band indicated with an asterisk, *. The β parameters were determined by using Equation 2, and the error bars due to counting statistics for the β values are typically ±0.03.

Figure 5 shows an expansion of the region of the on- and off-resonance spectra of the (I $4d_{5/2}^{-1}$)σ* resonance for binding energies between 8.6 and 11.2 eV, which includes the first four photoelectron bands. The spectra have been normalized to the intensity of the $\widetilde{A}\,^2A_2 \leftarrow \widetilde{X}\,^1A_1$ origin band, and Figure 5 also shows the on – off difference spectrum. The choice of the $\widetilde{A}\,^2A_2 \leftarrow \widetilde{X}\,^1A_1$ band will be justified in more detail below, but normalizing to other features results in a negative signal in the difference spectra for some of the bands. A non-zero signal in the latter reflects an increase in intensity from participator decay, but as a result of the normalization, participator decay to the vibrationless $\widetilde{A}\,^2A_2$ state will not be observed. The very small negative signals in the difference spectrum for some bands reflect a slight misregistration of the on- and off-resonance signals. While the on-resonance spectrum does show small enhancements for some of the bands, the overall shapes of the band envelopes remain unchanged. In particular, unlike the corresponding spectra for CH_3I,[10] no significant features are observed that can be directly associated with ionization as the C-I bond is stretching or breaking. This observation suggests that the autoionization process occurs before any significant change in molecular geometry.

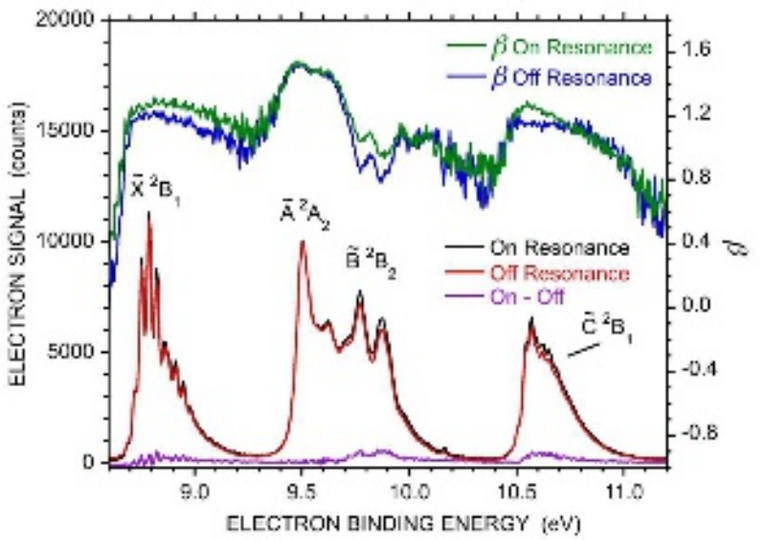

Figure 5. The first four electronic bands of the magic-angle photoelectron spectra of iodobenzene recorded on and off the (I $4d_{5/2}^{-1}$)σ* resonance (50.797 eV and 50.197 eV, respectively). The on – off difference spectrum is also shown, where the two spectra have been normalized to the intensity of the $\tilde{A}\ ^2A_2 \leftarrow \tilde{X}\ ^1A_1$ origin band. Also shown are the on- and off-resonance β parameters, which have typical error bars associated with the counting statistics of ±0.03.

The spectra recorded at other photon energies between 50 and 57 eV show similar behavior for these four bands, with relatively small contributions from the resonant participator processes. Figure 5 does imply a smaller enhancement for the $\tilde{A}\ ^2A_2 \leftarrow \tilde{X}\ ^1A_1$ band than for the other three bands, and this behavior is also observed at most of the other photon energies studied. Theoretical calculations by Palmer et al.[29] of the $3b_1$, $6b_2$, and $2b_1$ orbitals associated with the $C_6H_5I^+$ $\tilde{X}\ ^2B_1$, $\tilde{B}\ ^2B_2$, and $\tilde{C}\ ^2B_1$ states show significant electron density on the I atom, while the $1a_2$ orbital associated with the $\tilde{A}\ ^2A_2$ state has negligible electron density on the I atom. Thus, the lack of enhancement of the $\tilde{A}\ ^2A_2$ band from participator decay is consistent with the localization of the 4d hole on the I atom, and the expectation that participator processes involving orbitals with significant electron density on the I atom will be enhanced. Figure 5 also shows the on- and off-resonance photoelectron angular distribution parameters. Note that these parameters can be directly compared without any normalization. Figure 5 shows a clear increase in the on-resonance β values across the $\tilde{X}\ ^2B_1$, $\tilde{B}\ ^2B_2$, and $\tilde{C}\ ^2B_1$ bands relative to the off-resonance values, while no change in the β values are observed across the $\tilde{A}\ ^2A_2$ band. This difference clearly supports the conclusion that the participator processes involving the $1a_2$ orbital are significantly

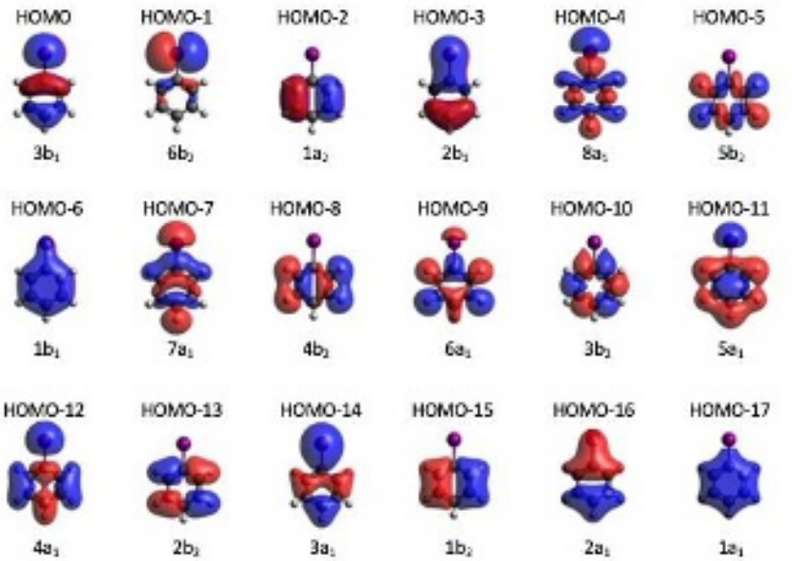

Figure 6. Images of the molecular orbitals of neutral ground state iodobenzene.

weaker than those involving the $3b_1$, $6b_2$, and $2b_1$ orbitals, and justifies our use of the $\tilde{A}\ ^2A_2$ band intensity for the normalization procedure.

The first 18 molecular orbitals for neutral C_6H_5I from our calculations are illustrated in Figure 6. The results are consistent with the results of Palmer et al.[29] for the first four orbitals. Note that, as in the earlier work, the ordering of the HOMO-1 and HOMO-2 flips between the neutral and the ion so that, in the ion, the $6b_2$ binding energy is higher than that of the $1a_2$ orbital. A similar reordering of the orbitals occurs for the HOMO-9 and HOMO-10.

Figure 7 shows the on- and off-resonance spectra for the C_6H_5I $(I\ 4d_{5/2}^{-1})\sigma^*$ resonance for electron binding energies between 11 and 16 eV, along with the corresponding difference spectrum. As in the lower binding energy spectra, there are only small differences between the on- and off-resonance spectra, and the shapes of the bands do not change significantly. The corresponding photoelectron angular distributions also show significantly smaller differences for the on- and off-resonance cases. This observation suggests that the participator processes are weaker for these bands than for the $\tilde{X}\ ^2B_1$, $\tilde{B}\ ^2B_2$, and $\tilde{C}\ ^2B_1$ bands. The small differences between the on- and off-resonance spectra in Figure 7 are all consistent with participator decay to single-hole states of the ion, and there is no obvious evidence for spectator decay to two-hole one particle states until above 15 eV in binding energy.

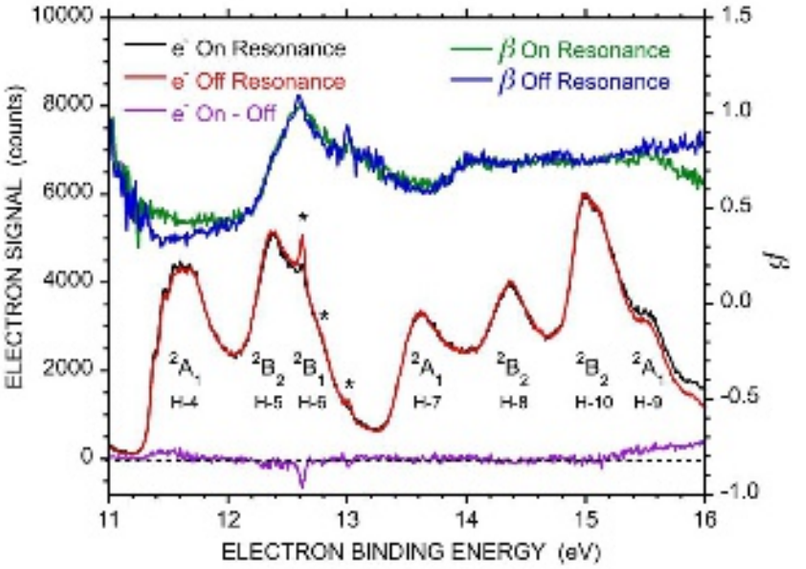

Figure 7. An expanded portion of the electron spectra and β parameters plotted in Figure 4. The on – off difference spectrum for the electrons is also shown, where the two spectra have been normalized to the intensity of the $\tilde{A}\ ^2A_2 \leftarrow \tilde{X}\ ^1A_1$ origin band. The H-n labels indicate the HOMO-*n* orbital for reference to Figure 6. The peaks labeled with an asterisk are due to an H_2O impurity that was greater for the off-resonance spectrum.

Figure 6 indicates that HOMO-4 has significant electron density on the I atom, and the corresponding feature does show up in the difference spectrum in Figure 7. The HOMO-7 has somewhat smaller, but still significant, electron density on the I atom, but a corresponding feature does not appear in the difference spectrum. Indeed, the only other significant feature in the difference spectrum appears at about the energy of the $^2A_1$ HOMO-9 band. However, the β parameter for this feature *decreases* relative to the β parameter in the off-resonance spectrum, while the β parameters for all of the other participator processes *increase* on resonance. This observation suggests that the feature appearing at ~15.5 eV is associated with a spectator, rather than participator, decay process. This process is discussed in more detail in the next section.

B. Spectator Decay Processes

Figure 8 shows an expanded portion of the on-resonance C_6H_5I (I $4d_{5/2}^{-1}$)σ^* photoelectron spectrum of Figure 4 for binding energies between 14.5 eV and 30 eV. The on- and off-resonance data show significant differences across this region. The corresponding data for the C_6H_5I (I $4d_{3/2}^{-1}$)σ^* photoelectron spectrum are quite similar. For electron binding energies above 25 eV,

the on-resonance electron spectrum increases considerably relative to the off-resonance data. This effect is a result of the rapidly increasing density of electronic states of $C_6H_5I^{2+}$, and thus an increasing density of the two-hole, one-particle states that can be populated by spectator decay.

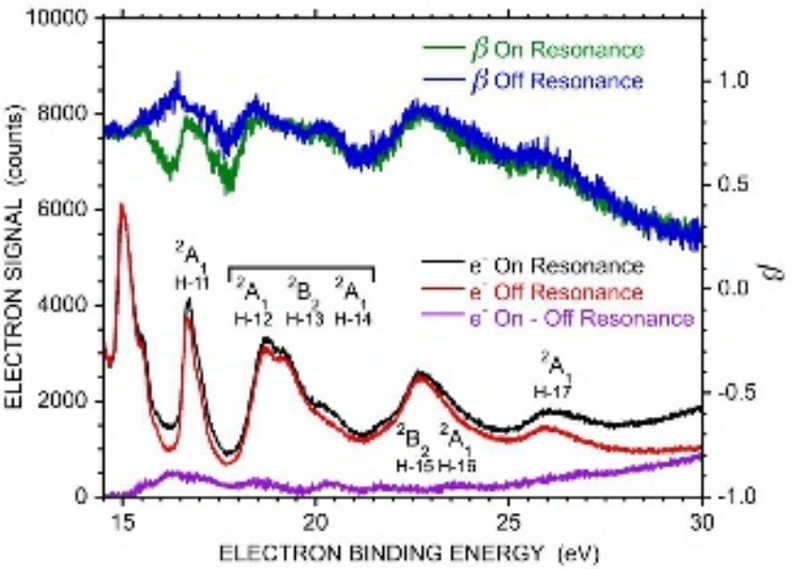

Figure 8. An expanded portion of the electron spectra and β parameters plotted in Figure 4. The on – off difference spectrum for the electrons is also shown, where the two spectra have been normalized to the intensity of the $\tilde{A}\ ^2A_2 \leftarrow \tilde{X}\ ^1A_1$ origin band.

In Figure 8, the most noticeable features in the difference spectrum and the angular distribution parameters are observed between 15 eV and 18 eV, as was evident in Figure 7. In particular, the on-resonance spectrum has considerable electron signal in the wings of the $^2A_1$ HOMO-11 feature, and this produces a relatively intense broad feature in the difference spectrum. The corresponding β parameter shows a strong dip in the wings of this feature. As discussed above, the β value for participator decay is observed to increase relative to the off-resonance value, suggesting that this feature in Figure 8 is due to a spectator process. The β values at the minima in the lower and higher energy wing of the $^2A_1$ HOMO-11 feature are 0.58 ± 0.03 and 0.53 ± 0.03, respectively. Figure 2 shows that the corresponding β values for true Auger decay of $C_6H_5I^+$ (I $4d^{-1}$) to the lowest levels of $C_6H_5I^{2+}$ are ~0.25 – 0.50. Because spectator decay involves the Auger decay of the $C_6H_5I^+$ ($4d^{-1}$) state, albeit in the presence of a σ* electron spectator, the similarity of the β values supports the assignment as spectator decay.

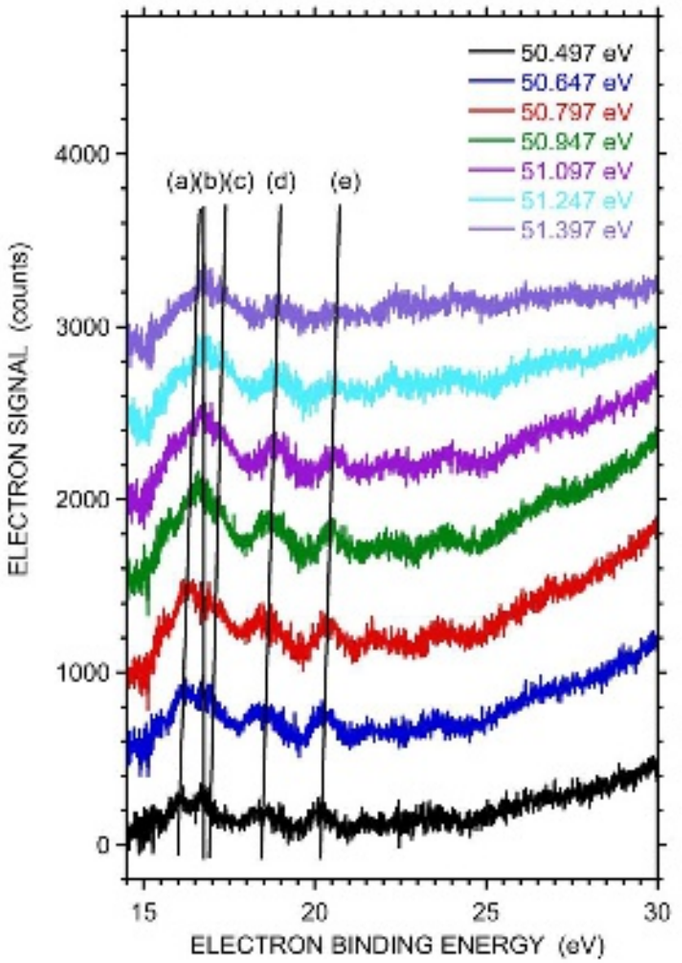

Figure 9. The on – off resonance magic-angle electron spectra for a series of excitation energies across the iodobenzene (I $4d_{5/2}^{-1}$)σ* resonance, as shown in the key. The magic-angle spectrum recorded at 49.966 eV was used as the off-resonance spectrum. The y-scale of each spectrum is offset from the one below it by 500 counts. The black lines are not fits, but are shown only to guide the eye.

The on-resonance β parameter in Figure 8 increases at the center of the $^2A_1$ HOMO-11 band. This observation suggests that participator decay is also important in this region. Indeed, as seen in Figure 6, the HOMO-11 does show significant electron density on the I atom. Note, however, that the final state populated at this electron binding energy by the participator and spectator processes is not the same, as the participator process is expected to populate the single-hole, $^2A_1$ HOMO-11 state, while the spectator process is expected to populate a two-hole, one-particle state.

Figures 9 and 10 illustrate this in more detail. These figures show the magic-angle difference spectra as a function of binding energy as the excitation energy is stepped across the C_6H_5I (I $4d_{5/2}^{-1}$)σ* and C_6H_5I (I $4d_{3/2}^{-1}$)σ* resonances, respectively, using the data at an excitation energy of 49.966 eV for the off-resonance spectrum. Between binding energies of 15 and 17 eV, each of the spectra in Figure 9 shows a broad feature, which in some cases splits into two, or even three

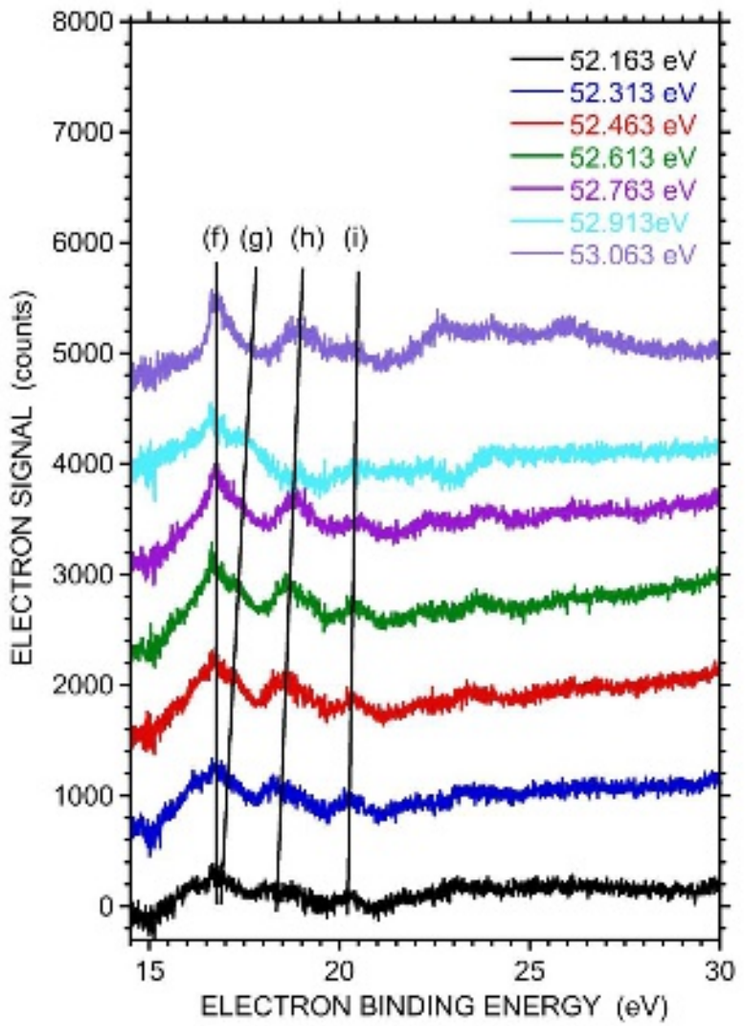

Figure 10. The on – off resonance magic-angle electron spectra for the series of energies across the iodobenzene (I $4d_{3/2}^{-1}$)σ* resonance, as shown in the key. The magic-angle spectrum recorded at 49.966 eV was used as the off-resonance spectrum. The y-scale of each spectrum is offset from the one below it by 800 counts. The black lines are not fits, but are shown only to guide eye.

partially resolved features. One component (b) of this feature appears to have a relatively constant binding energy of ~16.80 eV, while the second component (c) increases in energy with increasing photon energy. This behavior is repeated, somewhat more clearly, for the C_6H_5I (I $4d_{3/2}^{-1}$)σ* resonance in Figure 10. The constant energy feature (f), at the energy of the off-resonance $^2A_1$ HOMO-11 feature, is produced by participator decay, while the photon-energy dependent feature (g) is produced by spectator decay to a two-hole, one-particle state, most likely with a ($C_6H_5I^{2+}$)σ* configuration. As discussed for CH_3I previously, the energy-dependence arises from autoionization from the repulsive wall of the C_6H_5I (I $4d^{-1}$)σ* state to the repulsive wall of the ($C_6H_5I^{2+}$)σ*. If these two potential energy surfaces were parallel, the electron kinetic energy would remain constant, and the effective binding energy would increase linearly with increases in the photon energy. However, if the

repulsive walls have different slopes, the effective binding energy will show a photon energy dependence depending on the relative slopes. In the present case, the slope of this energy dependence of the binding energy is positive, suggesting that the slope of the $(C_6H_5I^{2+})\sigma^*$ surface is not as steep as that of the C_6H_5I (I $4d^{-1}$)σ^* surface.

Figures 9 and 10 show several additional peaks that have a positive photon energy dependence, and that are assigned to spectator decay. Note that the number of relatively low-lying states of $C_6H_5I^{2+}$ grows quickly with increasing energy, resulting in a large number of possible $(C_6H_5I^{2+})\sigma^*$ states.

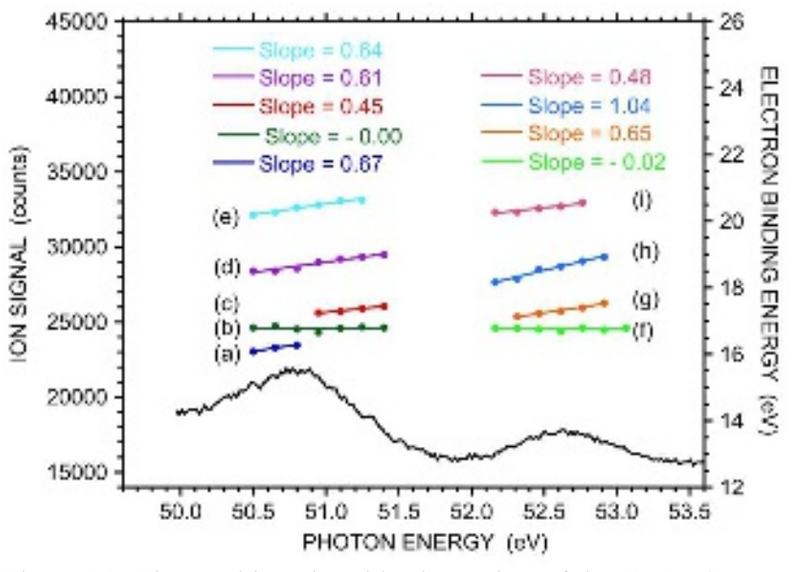

Figure 11. The total ion signal in the region of the C_6H_5I (I $4d_{5/2,3/2}^{-1}$)σ^* resonances. Also shown are the peak positions (electron binding energies) from Figures 9 and 10 at the photon energies of the series of spectra. The binding energies as a function of photon energy are fit by a linear function, with the slopes indicated.

Figure 11 shows the total ion yield vs. photon energy, along with the electron binding energies of the features observed in the electron binding energy spectra of Figures 9 and 10. The photon energy dependence of each feature is fit to a linear function, and the slope is indicated in the figure. For most of the features, the slope of the energy dependence is ~1 or less, suggesting that the slope of the $(C_6H_5I^{2+})\sigma^*$ final state surface is not as steep as that of the (I $4d^{-1}$)σ^* surface. More detailed information on the (I $4d^{-1}$)σ^* and $(C_6H_5I^{2+})\sigma^*$ potential

surfaces, along with information on the low-lying electronic states of $C_6H_5I^{2+}$, is necessary to make a detailed assignment of these features.

IV. CONCLUSIONS

We have presented new data on the resonant Auger decay of iodobenzene excited in the region just below the I $4d^{-1}$ thresholds. This region includes the broad (I $4d_{5/2,3/2}^{-1}$)σ* resonances, as well as some sharper Rydberg state resonances. The σ* resonances show evidence for both participator and spectator Auger processes, and the electron angular distribution can be used with the electron binding energy spectra to distinguish between these processes. We note that in the present study, the on-resonance β value increases for participator processes and decreases for spectator processes. Although we do not have a rationalization for the increase in β for the participator decay, the β value for true Auger decay in Figure 2 is ~0.3, significantly lower than the average off-resonance values. Thus, for a true spectator decay process, the β value would also be expected to decrease from the off-resonance value, as is observed.

The iodobenzene results show both similarities and differences with the analogous results for methyl iodide.[28] While participator processes are important for both molecules, CH_3I shows significant signal associated with autoionization as the C-I bond in the resonant state is stretching/breaking,[10] while no such evidence is observed in iodobenzene. This observation may result at least in part from the slower separation of fragments in the heavier system. Both systems show considerable evidence for spectator decay processes that access the repulsive walls of two-hole, one-particle final states. Such states with the lowest energy lie around 15 to 17 eV, consistent with the similar double ionization energies of methyl iodide and iodobenzene. Accurate theoretical calculations of the relevant electronic state surfaces for C_6H_5I, $C_6H_5I^+$, and $C_6H_5I^{2+}$ are difficult, but would certainly be helpful in determining the detailed assignments and character of the final states.

V. ACKNOWLEDGEMENTS

We are grateful to the SOLEIL staff for running the facility and providing beamtime under Project No. 20200370. S.T.P. is supported by the U.S. Department of Energy, Office of Science, Office of Basic Energy Sciences, Division of Chemical Sciences, Geosciences, and Biosciences under contract No. DE-AC02-06CH11357. D.M.P.H. is grateful to the Science and Technology Facilities Council (United Kingdom) for financial support.

REFERENCE

1. P. Morin, M. Simon, C. Miron, N. Leclercq, E. Kukk, J. D. Bozek, and N. Berrah, Role of bending in the dissociation of selective resonant inner-shell excitation as observed in CO_2, Phys., Rev. A **61**, 050701(R), 2000.
2. I. Hjelte, M. N. Piancastelli, R. F. Fink, O. Björnholm, M. Bässler, R. Feifel, A. Giertz, H. Wang, K. Wiesner A. Ausmees, C. Miron S. L. Sorensen, and S. Svensson, Evidence for ultra-fast dissociation of water from resonant Auger spectroscopy, Chem. Phys. Lett. **334**, 151-158 (2001).
3. C. Miron, R. Feifel, O. Björneholm, S. Svensson, A. Naves de Brito, S. L. Sorenson, M. N. Piancastelli, M. Simon, and P. Morin, Mapping potential energy surfaces by core electron excitation: the resonant Auger decay spectrum of BF_3, Chem. Phys. Lett, **359**, 48-54 (2002).
4. O. Travnikova, E. Kukk, F. Hosseini, S. Granroth, E. Itälä, T. Marchenko, R. Guillemin, I. Ismail, R. Moussaoui, L. Journel, J. D. Bozek, R. Püttner, P. Krasnov, V. Kimberg, F. Gel'mukhanov, M. N. Piancastelli, and M. Simon, Ultrafast dissociation of ammonia: Auger Doppler effect and redistribution of the internal energy, Phys. Chem. Chem. Phys. **24**, 5842-5854 (2022).
5. O. Travnikova, F. Hosseini, T. Marchenko, R. Guillemin, I. Ismail, R. Moussaoui, L. Journel, A. Milosavljevic, J. D. Bozek, E. Kukk, R. Püttner, M. N. Piancastelli, and M. Simon, Dynamics of core-excited ammonia: disentangling fragmentation pathways by complementary spectroscopic methods, Phys. Chem. Chem. Phys. **25**, 1063-1074 (2023).
6. G. B. Armen, H. Aksela, T. Åberg, and S. Aksela, The resonant Auger effect, J. Phys. B **33**, R49-R92 (2000).
7. V. Schmidt, Electron Spectrometry of Atoms using Synchrotron Radiation (Cambridge University Press, Cambridge, U.K., 1997).

8. M. N. Piancastelli, Auger resonant Raman studies of atoms and molecules, J. Electron Spectrosc. Rel. Phenom. **107**, 1-26 (2000).
9. K. Kimura, S. Kasumata, Y. Achiba, T. Yamazaki, and S. Iwata, *Handbook of He I Photoelectron Spectra of Fundamental Organic Molecules* (Halsted Press, New York, 1981).
10. S. T. Pratt, U. Jacovella, B. Gans, J. D. Bozek, and D. M. P. Holland, Resonant Auger decay of dissociating CH_3I near the I 4d threshold. J. Chem. Phys.**160**, 074304 (2024).
11. P. Morin and I. Nenner, Atomic autoionization following very fast dissociation of core-excited HBr, Phys. Rev. Lett. **56**, 1913-1916 (1986).
12. P. Morin and C. Miron, Ultrafast dissociation: An unexpected tool for probing molecular dynamics, J. Electron Spectrosc. Rel. Phenom. **185**, 259-266 (2012).
13. E. Kukk, H. Aksela, O. -P. Sairanen, E. Nõmmiste, S. Aksela, S. J. Osborne, A. Ausmees, and S. Svensson, Core-to-Rydberg excitations and their Auger decay in the HCl and DCl molecules, Phys. Rev. A **54**, 2121-2126 (1996).
14. J. Söderström, A. Lindblad, A. N. Grum-Grzhimailo, O. Travnikova, C. Nicolas, S. Svensson, and C. Miron, Angle-resolved electron spectroscopy of the resonant Auger decay in xenon with meV energy resolution, New J. Phys. **13**, 073014 (2011).
15. K. Codling, R. P. Madden, and D. L. Ederer, Resonances in the photo-ionization continuum of Ne I (20-150 eV), Phys. Rev. **155**, 26-37 (1967).
16. K. Schultz, M. Domke, R. Püttner, A. Gutiérrez, G. Kaindl, G. Miecznik, and C. H. Greene, High-resolution experimental and theoretical study of singly and doubly excited resonances in ground-state photoionization of neon, Phys. Rev. A **54**, 3095-3112 (1996).
17. D. M. P. Holland, D. Edvardsson, L. Karlsson, R. Maripuu, K. Siegbarn, A. W. Potts, and W. von Niessen, A systematic investigation of the influence of Cooper minima on the photoionization dynamics of the monohalobenzenes, Chem. Phys. **253**, 133-155 (2000).

18. C. N. Yang, On the Angular Distribution in Nuclear Reactions and Coincidence Measurements, Phys. Rev. **74**, 764-772 (1948).
19. J. Cooper and R. N. Zare, Angular distribution of photoelectrons, J. Chem. Phys. **48**, 942-943 (1968).
20. K. Reid, Photoelectron Angular Distributions, Ann. Rev. Phys. Chem. **54**, 397-424 (2003).
21. I. Powis, D. M. P. Holland, E. Antonsson, M. Patanen, C. Nicolas, C. Miron, M. Schneider, D. Yu. Soshnikov, A. Dreuw, and A. B. Trofimov, The influence of the bromine atom Cooper minimum on the photoelectron angular distributions and branching ratios of the four outermost bands of bromobenzene, J. Chem. Phys. **143**, 144304 (2015).
22. Gaussian 16, Revision C.01, M. J. Frisch, G. W. Trucks, H. B. Schlegel, G. E. Scuseria, M. A. Robb, J. R. Cheeseman, G. Scalmani, V. Barone, G. A. Petersson, H. Nakatsuji, X. Li, M. Caricato, A. V. Marenich, J. Bloino, B. G. Janesko, R. Gomperts, B. Mennucci, H. P. Hratchian, J. V. Ortiz, A. F. Izmaylov, J. L. Sonnenberg, D. Williams-Young, F. Ding, F. Lipparini, F. Egidi, J. Goings, B. Peng, A. Petrone, T. Henderson, D. Ranasinghe, V. G. Zakrzewski, J. Gao, N. Rega, G. Zheng, W. Liang, M. Hada, M. Ehara, K. Toyota, R. Fukuda, J. Hasegawa, M. Ishida, T. Nakajima, Y. Honda, O. Kitao, H. Nakai, T. Vreven, K. Throssell, J. A. Montgomery, Jr., J. E. Peralta, F. Ogliaro, M. J. Bearpark, J. J. Heyd, E. N. Brothers, K. N. Kudin, V. N. Staroverov, T. A. Keith, R. Kobayashi, J. Normand, K. Raghavachari, A. P. Rendell, J. C. Burant, S. S. Iyengar, J. Tomasi, M. Cossi, J. M. Millam, M. Klene, C. Adamo, R. Cammi, J. W. Ochterski, R. L. Martin, K. Morokuma, O. Farkas, J. B. Foresman, and D. J. Fox, Gaussian, Inc., Wallingford CT, 2016.
23. Avogadro: an open-source molecular builder and visualization tool. Version 1.XX. http://avogadro.cc/.

24. Marcus D Hanwell, Donald E Curtis, David C Lonie, Tim Vandermeersch, Eva Zurek and Geoffrey R Hutchison; Avogadro: An advanced semantic chemical editor, visualization, and analysis platform, J. Cheminformatics **4**:17, 2012. *Journal of Cheminformatics* **2012**, 4:17.
25. J. N. Cutler, G. M. Bancroft, and K. H. Tan, Ligand-field splittings and core-level linewidths in 4d photoelectron spectra of iodine molecules, J. Chem. Phys. **97**, 7932-7943 (1992).
26. T. X. Carroll, J. D. Bozek, E. Kukk, V. Myrseth, L. J. Sæthre, T. D. Thomas, and K. Weisner, Xe N4,5OO Auger spectrum – a useful calibration source, J. Electron Spectrosc. Rel. Phenom. **125**, 127-132 (2002).
27. J. H. D. Eland and R. Feifel, *Double Photoionisation Spectra of Molecules* (Oxford University Press, Oxford, U.K., 2018).
28. R. Forbes, A. De Fanis, D. Rolles, S. T. Pratt, I. Powis, N. A. Besley, A. R. Milosaviljević, C. Nicolas, J. D. Bozek, and D. M. P. Holland, Photoionization of the I 4d valence orbitals of methyl iodide, J. Phys. B At. Mol. Opt. Phys. 53, 155101 (2020).
29. M. H. Palmer, T. Ridley, S. V. Hoffman, N. C. Jones, M. Coreno, M. de Simone, C. Grazioli, M Biczysko, and A. Baiardi, The ionic states of iodobenzene studied by photoionization and ab initio configuration interaction and DFT computations, J. Chem. Phys. 142, 134301 (2015).